Molecular Dynamics Simulation of Swollen Membrane of Perfluorinated Ionomer

Shingo Urata,* Jun Irisawa, and Akira Takada

Research Center, Asahi Glass Co., Ltd. (AGC), 1150 Hazawa-cho, Kanagawa-ku, Yokohama, Kanagawa 221-8755, Japan

Wataru Shinoda, Seiji Tsuzuki, and Masuhiro Mikami

National Institute of Advanced Industrial Science and Technology (AIST), 1-1-1 Umezono, Tsukuba, Ibaraki 305-8568, Japan

Received: August 9, 2004; In Final Form: December 13, 2004

Molecular dynamics simulations of the swollen membrane of perfluorinated ionomer, which is composed of poly(tetrafluoroethylene) backbones and perfluosulfonic pendant side chains, have been undertaken to analyze the static and dynamic properties of the water and the side chain in the membrane. The calculations were carried out for four different water contents, 5, 10, 20 and 40 wt %, at 358.15 K and 0.1MPa.The results are summarized as follows: (1) The sulfonic acid is the unique site to which water molecules can bind, and the other sites in the pendant side chain have no bound water even at high water concentration. (2) Sulfonic acids aggregate in the short range within 4.6−7.7 Å despite the electrostatic repulsion between them. In such aggregates, a water molecule bridges two sulfonic acids. (3) Pendant side chains prefer to orient perpendicular to the hydrophilic/hydrophobic interface, and long-range correlation of side chain orientations is observed at 20 and 40 wt % water uptake membranes. (4) In a low water uptake membrane, the dynamics of water is substantially restricted due to strong attractive interactions with acidic sites. In contrast, at high water content, even the water locating near the sulfonic acid is relatively mobile. The short residence time of the bound water reveals that such water can frequently exchange position with relatively free water, which locates in the center of water cluster, in highly swollen membranes.

Introduction

The perfluorinated ionomers composed of poly(tetrafluoroethylene) backbones with perfluorinated pendant chains terminated by sulfonic acid, such as Flemion,[1] Nafion,[2] and Aciplex[3] (Figure 1), have been widely utilized in various industrial applications.[4] Especially, they have attracted much attention as proton exchange membranes in the polymer electrolyte fuel cells, because the swollen membranes of these polymers have high proton conductivity. Because the proton conductivity substantially depends on the water uptake ratio into the membrane[5−9] and dissociated protons are thought to conduct through the water path, it is important to understand the static and dynamic properties of the water molecules contained in the membrane. Commonly, the water path is thought to be composed of about several nanometer sizes of water clusters connected with 1 nm channels (cluster network model).[4,10,13] The small-angle X-ray[11−21] and neutron scattering[14,17] (SAXS and SANS, respectively) estimate that the size of the water clusters is 3−5 nm, and several models of the water aggregation in the membranes have been proposed. One of the models is the two-phase paracrystalline model that relates the Bragg spacing with the ordered intercluster interference.[13] The other is the core−shell model. In the latter model, the Bragg spacing is assumed to reflect a short-range order distance associated with the size of the core−shell, which contains most of the sulfonic acid groups.[11,12] Additionally, several modified models have been proposed.[4,15] The morphology the of swollen membrane has also been visualized using scanning force microscopy,[22] transmission electron microscopy,[21] and atomic force microscopy.[18,19] In addition, computer simulation techniques such as dissipative particle dynamics,[23] Monte Carlo simulation combined with reference interaction site model,[24] bond-fluctuation-method,[25] and self-consistent mean field theory[26] have been extensively used to understand the morphology of swollen membranes. Paddison and co-workers have extensively studied proton transfer and side chain conformation with bound water by using molecular orbital (MO) calculations and theoretical modeling.[27−32] To understand the structure of the membrane and the water dynamics at the molecular level, several experimental measurements have been undertaken by using nuclear magnetic resonance (NMR),[33−35] differential scanning calorimetry,[36] dielectric relaxation,[37−40] and infrared spectroscopy.[41,42] However, our understanding on the water properties inside the membrane is still quite limited. Molecular simulation techniques, such as molecular orbital[43] and molecular dynamics (MD) calculations,[44−48] are also useful tools to investigate local microstructure and micro-dynamics of molecular systems. These methods provide additional information, which cannot be obtained by experimental investigations. In this study, we therefore try to

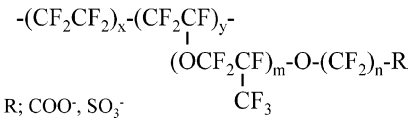

Figure 1. Schematic illustration of perfluorinated ionomers. Flemion: $m = 0-1$, $n = 1-5$. Nafion: $m = 1$, $n = 1$. Aciplex: $m = 0-2$, $n = 1-4$. (See ref 4.)

* Corresponding author. Tel: +81−045-374-7074. Fax: +81−045-374-8730. E-mail: shingo-urata@agc.co.jp.

10.1021/jp046434o CCC: $30.25
Published on Web 02/10/2005

TABLE 1: Summary of Simulation Conditions

		5 wt %	10 wt %	20 wt %	40 wt %
no. of molecules					
polymer		80	30	40	10
H_2O		1433	1468	4902	3435
H_3O^+		800	300	400	100
total no. of particles		24299	11904	24706	12805
simulation time		2.5ns	1.3ns	1.4ns	1.3ns
H_2O/SO_3		2.8	5.9	13.3	35.4
av cell size (Å)		83.1	62.2	74.9	56.2
density	calc	2.08	1.97	1.72	1.39
	expt[a]	1.95	1.87	1.74	1.58
	error (%)	6.0	5.1	−1.5	−13.4

[a] References 49 and 50.

analyze the local information on polymer and water in perfluorinated ionomes with 5−40 wt % water contents by using MD simulations. Although Vishnyakov and Neimark have already carried out MD simulations of a Nafion oligomer in water,[44] methanol and water−methanol mixture,[45] and 5.0, 12.5, and 17.0 wt % water contents of swollen membranes of Nafion,[46] their simulation scale, using only fifteen 10-unit olygomers, is not large enough to study the nanometer sized hydrophilic clusters.[46] In this report, on the basis of larger scale molecular dynamics simulations, we present several new information on the static and dynamics of ionomer and water therein. What we have done here is (1) larger simulation systems are studied, and long-range organization of water cluster is reproduced, consistent with experiments, (2) our simulations also demonstrate several nanometer periodicity of sulfonic acids, (3) water content dependence of microscale aggregation of sulfonic acids and water coordination along the pendant side chain are investigated, and (4) translational and rotational dynamics of water depending on water content ratio and also on water location are discussed in detail.

Computational Method

Isobaric−isothermal ensemble MD simulations were carried out for 5, 10, 20, and 40 wt % water content membranes (see Table 1) of perfluorinated inomer by using the molecular simulation program, *MPDyn*, developed by Shinoda.[51] It is assumed that one polymer consists of 10 monomers, which are composed of 16 CF_2 groups in the main chain ($x = 7$, $y = 1$), and $m = 1$, $n = 2$ are assumed for sulfonic type pendant chain in Figure 1. (This model is the same with the model used in refs 44−46 for Nafion.) Then, CF_3, CF_2, and CF are modeled as united atoms to reduce computational costs. It has already been revealed that such a superatom model can reasonably reproduce the properties, such as liquid density, critical properties, and vapor−liquid equilibrium of the perfluorocarbones[52,53] and perfluoroethers.[54] The water molecule and sulfonic acid are treated as all-atom models. The flexible TIP3P model[55,56] was applied for water. To keep the neutrality of the system, H_3O^+ is used as counterion of sulfonic acids. The fractional charges, which were determined by MO calculation at the B3LYP/6-31+G* level[57−60] with ChelpG method,[61] on hydrogen and oxygen for this counterion were $+0.518q$ and $-0.554q$, respectively. Force constants of O−H bonding and H−O−H bending were assumed to be the same with those of modified TIP3P water, and an improper torsion potential was assign to keep the geometry. We will not take proton transfer into account in this study; however, we suppose that this assumption would not affect much the results in this article, so long as we focus on average behavior of water.

Intermolecular interactions were modeled with the Lennard-Jones (LJ) potential and the Coulombic interaction. The Ewald

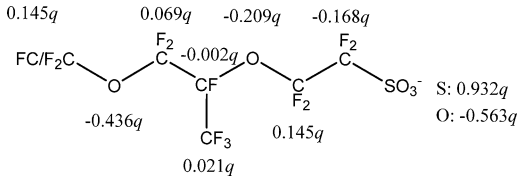

Figure 2. Fractional charges evaluated at the B3LYP/6-31+G* with ChelpG method for pendant chain.

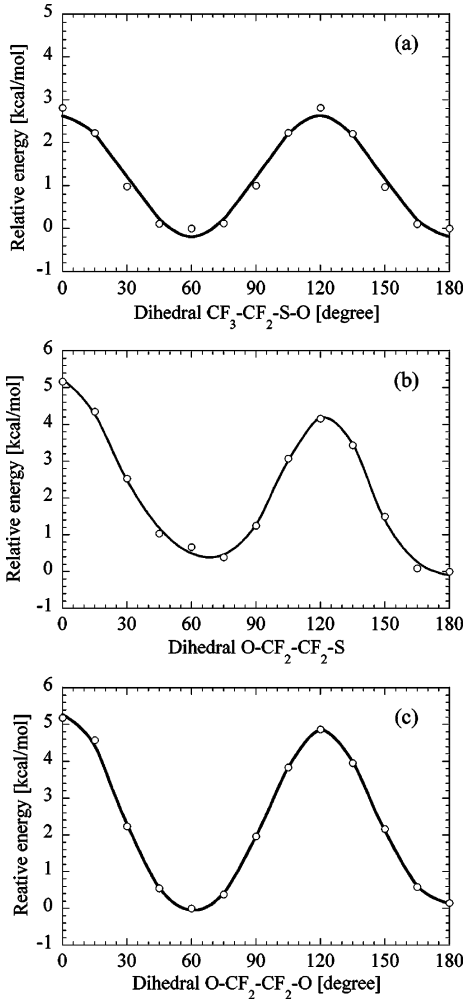

Figure 3. Fitting results on torsion potentials for (a) CF_3-CF_2-S-O, (b) $O-CF_2-CF_2-S$, and (c) $O-CF_2-CF_2-O$.

method[62] was used for the calculation of the coulomb interaction. The partial charges, which were determined by MO calculation at the B3LYP/6-31+G* level with the ChelpG method, were located on each site on pendant chain, and those for united atoms were assumed to be summations of the values of constituent atoms, respectively. These values are shown in Figure 2. On the contrary, sites on backbones were set to be neutral. This is the same as the models for perfluorinated molecules.[52−54] The above assumption is thought to be acceptable, because such a model can reasonably reproduce the vapor−liquid equilibrium of perfluorinated molecules, and also our MO calculation studies have revealed that the intermolecular interaction between the CF_3 group of $CF_3OCF_2CF_2SO_3^-$, which is a model of the pendant side chain, and water molecule is only −2.25 kcal/mol at the MP2/aug-cc-pVDZ//B3LYP/6-31+G* level. That is substantially smaller than that between sulfonic acid group and water (−10.58 kcal/mol).[43,63] For the all-atom model, the OPLS-AA force field[64] was applied to the Lennard-Jones, bonding, angle, and torsion potentials. Here, we determined the equilib-

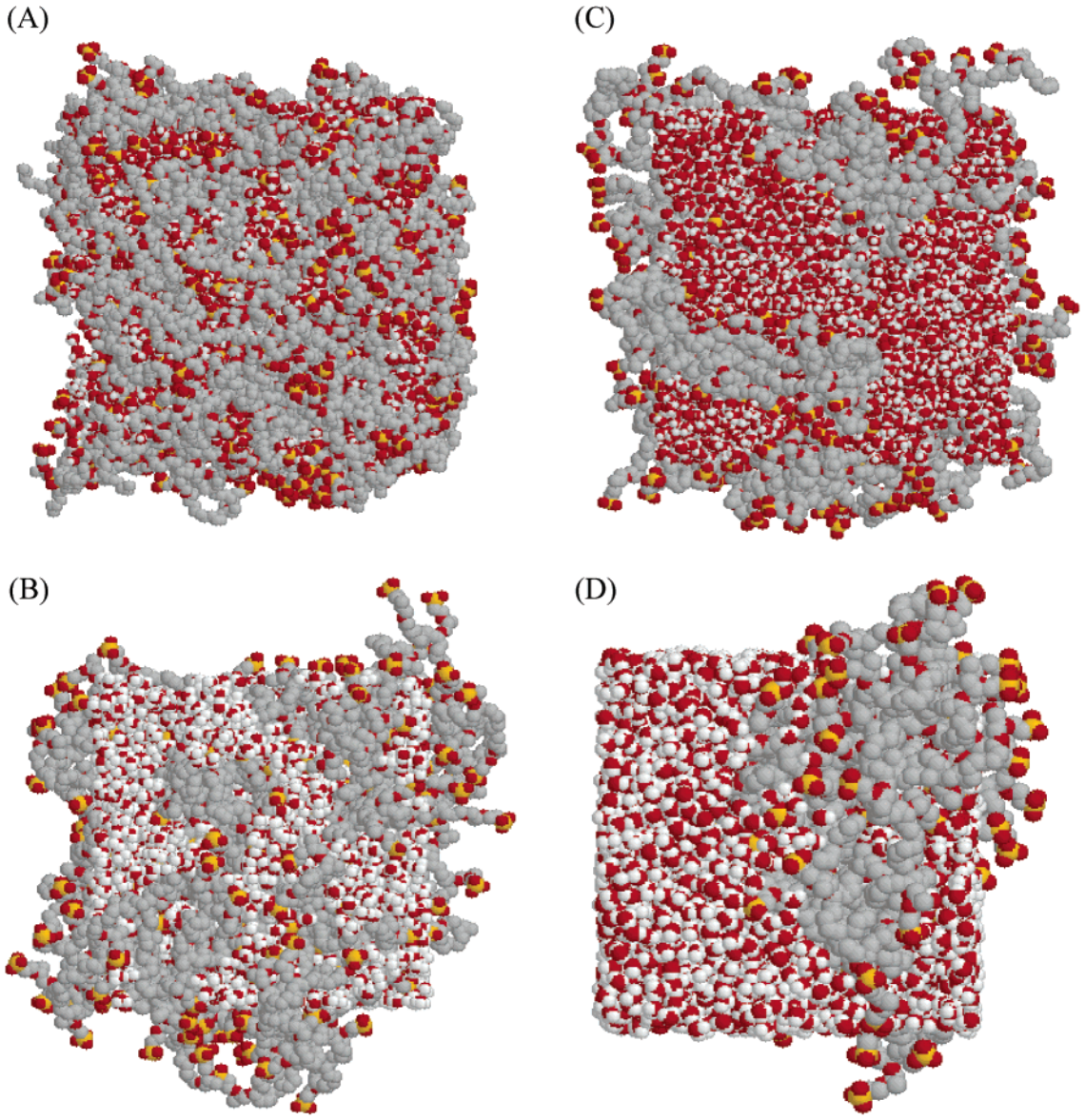

Figure 4. Final snapshots of MD simulations for (A) 5 wt %, (B) 10 wt %, (C) 20 wt %, (D) 40 wt %. Colors: red, oxygen atoms of water, H_3O^+, and sulfonic acid; gray, CF_x groups ($x = 1-3$); yellow, sulfur; white, hydrogen.

TABLE 2: Optimized Parameters (V_i) of Torsion Potentials: O−CF_2−CF_2−S, CF_2−CF_2−S−O, and O−CF_2−CF_2−O (kcal/mol)

dihedral	function type	$i=0$	$i=1$	$i=2$	$i=3$	$i=4$	$i=5$	$i=6$	$i=7$
O−CF_2−CF_2−S	polynomial	7.5006	−5.4317	8.1808	7.8136	−20.2827	4.7371	13.1162	−3.6935
CF_2−CF_2−S−O	fourier		2.1227	−2.2593	0.9470				
O−CF_2−CF_2−O	polynomial	3.5663	−6.8616	2.2128	9.3309	−6.3254	1.1900	4.5396	−0.8555

rium lengths of S−O and CF_2−S bonds and equilibrium angles of CF_2−S−O, O−S−O, and CF_2−CF_2−S at the MP2/6-31+G* level[65] of ab initio calculation of $CF_3CF_2SO_3^-$ because several potential parameters are absent for the sulfonic acid group. The force constant parameters of these bond stretching and angle bending were assumed as the same as those of C−C bond[64] and CF_2−CF_2−O angle,[54] and Lennard-Jones parameters of the sulfonic oxygen were taken from those of the ether oxygen.[64] The models of Cui et al.[52,53] and Li et al.[54] are utilized for those parameters of united atoms. LJ interaction and real-space Ewald terms were truncated at 10 Å. Long-range energy correction was taken into account. Here, because torsion potentials for several dihedral angles, such as CF_2−CF_2−S−O, O−CF_2−CF_2−S, and O−CF_2−CF_2−O, have not yet been reported, we constructed potential models for them on the basis of the ab initio calculations of $CF_2CF_2SO_3^-$, $CF_3OCF_2CF_2SO_3^-$, and CF_3-$OCF_2CF_2OCF_3$, respectively. The first molecule was calculated at the MP2/6-31+G*, and the others were done at the MP2/6-31+G*//HF/6-31+G* level.[65] Potential parameters of O−CF_2−CF_2−S and O−CF_2−CF_2−O dihedrals were fit as a polynomial-type function of cos ϕ

$$E_{\text{torsion}}^{\text{poly}} = \sum_{i=0}^{7} V_i \cos^i \phi \qquad (1)$$

and those of CF_2−CF_2−S−O were parametrized using Fourier series as follows:

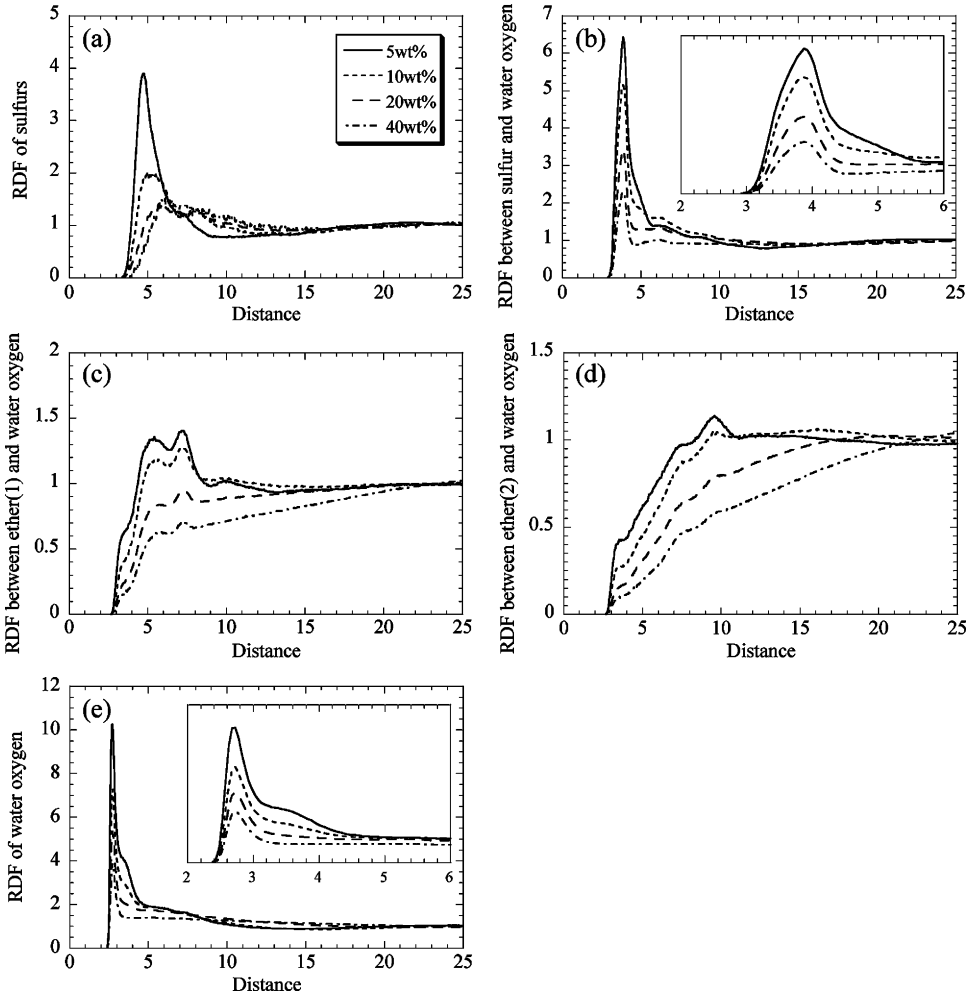

Figure 5. Radial distribution functions (RDFs) evaluated from MD simulations: (a) sulfur; (b) sulfur and water oxygen; (c) water oxygen and ether near sulfonic acid; (d) water oxygen and ether far side from sulfonic acid; (e) water oxygen.

$$E_{\text{torsion}}^{\text{Fourier}} = \frac{1}{2}[V_1(1 + \cos\phi) + V_2(1 - \cos 2\phi) + V_3(1 + \cos 3\phi)] \quad (2)$$

where ϕ is dihedral angle. The fitted results and optimized parameters are presented in Figure 3 and Table 2, respectively. In the fitting procedure, electrostatic, and Lennard-Jones interactions between intramolecular sites separated less than four bonds and less than three bonds were omitted when polynominal-type and Fourier series torsional terms work, respectively. Molecular orbital calculations were performed by using Gaussian 98 suite of programs.[66]

All MD simulations were performed at 358.15 K and 0.1 MPa with periodic boundary condition. Andersen method[67] was utilized for pressure control, and the Nosé−Hoover chain[68] was used as a thermostat of the system. Integration of the equations of motion was carried out by using the rRESPA algorithm[69] with multiple time steps: The time step used for the update of the Ewald reciprocal forces was 2.0 fs, the update of the real space nonbonded forces was 1.0 fs, and the update of the intramolecular interactions occurred every 0.2 fs. Total 2.5, 1.3, 1.4, and 1.3 ns intervals of MD simulations were performed for 5, 10, 20, and 40 wt % swollen membranes, respectively, and the final 300 ps trajectories of each simulation (6000 configurations) were used for the analyses. Conditions of the investigated systems are summarized in Table 1.

Results and Discussion

A. Local Structure around Side Chain. The final snapshots of four MD runs (Figure 4) and the radial distribution functions (RDFs) of sulfur (Figure 5) clearly reveal that the sulfonic acids localize in a small domain despite electrostatic repulsion between them. One sulfonic acid can be found within the range of 4.6, 5.6, 6.6, and 7.7 Å from another sulfonic acid for 5, 10, 20, and 40 wt % swollen membranes, respectively; the distance between sulfonic acids is gradually increased with increasing water content. Figure 6a shows the static structure factors evaluated by the Fourier transform of the RDF profiles of sulfur as defined below;

$$S(q) = 1 + 4\pi\frac{N}{V}\int[g(\mathbf{r}) - 1]\frac{\sin(qr)}{q}r\,\mathrm{d}r \quad (3)$$

A broad peak around 1.5 Å^{-1} at 5 wt % swollen membrane corresponds to the 3−5 Å periodicity of sulfonic acids. This peak position systematically shifts to smaller q value with increase of water content, which implies separation of sulfonic acids, probably as a result of water cluster growth due to water uptake.

On the other hand, another clear peak exists around the 0.3 Å^{-1} range that represents about 20 Å periodicity of the acidic sites. Although the peak intensity decreases with increasing water uptake ratio, the peak is observed even in a highly swollen membrane, i.e., over 20 wt % water uptake. A possible reason for this peak is an artifact of the polymer model because the

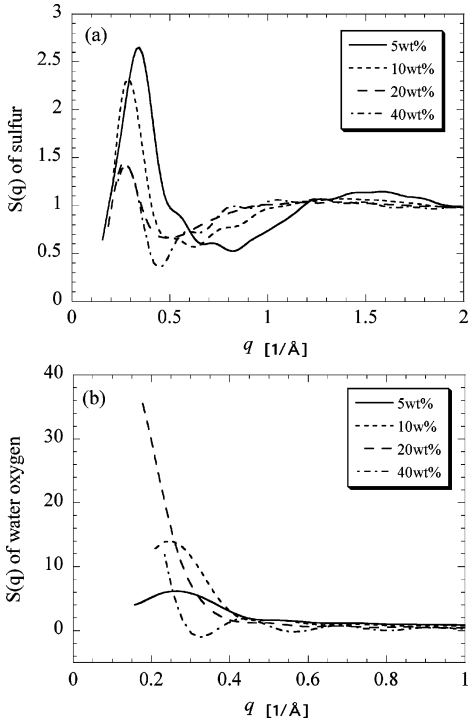

Figure 6. Structure factors estimated as Fourier transform of RDFs for (a) sulfur and (b) water oxygen.

side chains are placed at even intervals of sixteen carbon atoms in our simulation. To check the effect of this periodicity, the structure factors were calculated from the RDFs, which were evaluated with eliminating the contribution from the sulfurs in the same polymer chain. As a result, almost the same profiles of structure factors as Figure 6a were obtained for all humidity conditions. Therefore, the interval of pendant side chains should be unaccountable to the peak around 0.3 $Å^{-1}$. This result provides us a possible situation that a few nanometers size of water channels exist in the membranes even at high water concentration, although it is difficult to distinguish the contribution from the periodicity of polymers' aggregation.

Coordination numbers of water around sulfonic acids, which were calculated from the RDFs (Figure 5) shorter than 4.5 Å, are 4.9, 6.5, 7.2, and 7.5 waters for 5, 10, 20, and 40 wt % swollen membranes, respectively (H_3O^+ included). Reversely, the numbers of sulfonic acids, which were found within 4.5 Å from a water molecule, are 1.5, 1.0, 0.5, and 0.4 sulfurs for 5, 10, 20, and 40 wt % systems; therefore, we can recognize that a water molecule should be shared by several sulfonic acids in less than 10 wt % water content membrane. Figure 7 displays the water coordination numbers evaluated from the RDFs within 4.5 Å along the side chain (H_3O^+ included). It is possible to see that water highly concentrates to the headgroup, SO_3^-, and the water coordination numbers exponentially decrease as a function of distance from sulfonic acid at all humidity conditions. This phenomenon implies that only the sulfonic acid can preferably bind with water, and the tail end of side chain holds few water molecules even at relatively high water content conditions, such as 20 and 40 wt % swollen membranes. From these data, we can presume such a situation that only sulfonic acid groups associate with a water cluster, and they thus locate on the surface of that cluster. This picture is in accord with the previous study[46] and will support the water cluster models proposed by experimental studies:[4,10,13,20] for example, Rollet et al. has observed that $N(CH_3)^{4+}$ ions are condensed at the interface between hydrophilic and hydrophobic phases when the hydrated membrane is neutralized by the counterion.[20]

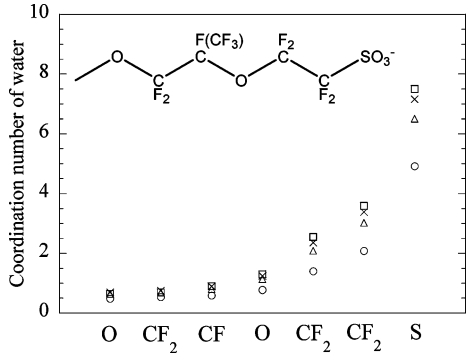

Figure 7. Water coordination numbers along the side chain evaluated from the RDFs until 4.5 Å. Circle, triangle, cross, and square are 5, 10, 20, and 40 wt % water swollen membranes, respectively.

TABLE 3: Proton Affinities of CH_3OCH_3, CF_3OCH_3, and CF_3OCF_3[a]

electron correlation correction method	basis set	proton affinity (kcal/mol) CH_3OCH_3	CF_3OCH_3	CF_3OCF_3
B3LYP	6-31++G**[b]	188.3	157.6	136.1
MP2	6-31G*	187.3	158.0	136.5
	6-31++G**	189.1	157.0	134.6
	6-311+G**	189.1	158.7	137.8
	6-311++G**	189.2	158.8	137.9
	aug-cc-pVDZ	186.3	156.5	135.0
	aug-cc-pVTZ	186.8	158.2	
MP3	6-31G*	189.2	158.6	134.8
MP4(DQ)	6-31G*	189.5	159.1	135.5
MP4(SDQ)	6-31G*	189.3	159.4	136.8
CCSD(T)	6-31G*	188.9	159.4	
Expt.[c]		189.3	171.9	

[a] Geometries and thermal corrections for enthalpy were calculated at the B3LYP/6-31++G** level. [b] Energies were taken from ref 73. [c] Reference 72.

It is also interesting to note that two ether oxygen atoms in the side chain cannot hold sufficient numbers of water, even though they typically play as proton acceptor. According to the RDF profiles between two ethers and water, the ether closer to the sulfonic acid has a broad peak around 7 Å, whereas the other one has its peak around 10 Å, as seen in Figure 5. These peaks represent that the water directly coordinates to the sulfonic acid, but not to ether oxygen atoms. The hydrophobic behavior of ethers might be due to the electron withdrawing effect by fluorination, because it has been demonstrated that fluorination substantially reduces proton acceptability of ether oxygen.[70,71] In fact, our previous ab initio study, which investigated the intermolecular interaction between $CF_3OCF_2CF_2SO_3^-$ and water,[43] has shown that the water locating near ether oxygen is by about 5.0 kcal/mol less stabilized than that near sulfonic acid. Additionally, both experimental and theoretical investigations have shown that fluorination substantially reduces the proton affinity (PA) of ether oxygen as shown in Table 3.[72,73] Note here that there is a large discrepancy between the experimental and theoretical PA values for CF_3OCH_3. To check it, we estimated both basis set size and electron correlation effects on the PA calculation (see Table 3). Consequently, the larger basis set and higher level of electron correlation correction methods, such as coupled cluster calculations,[74] improve PA estimation; however, the difference from the experimental value is even large. Although we could not ensure the reason experimental and theoretical values for CF_3OCH_3 are so different, we believe the previous[73] and our calculations prove that fluorination substantially reduces the PA of the ether oxygen.

B. Pendant Side Chain Orientation. Next, we estimated pendant side chain directions against to the interface between

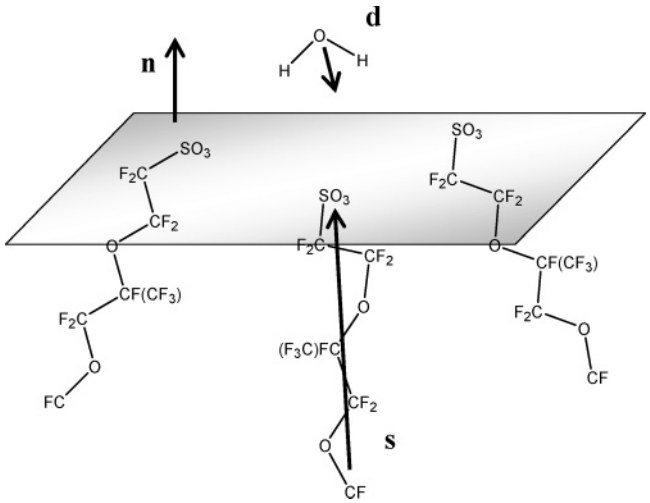

Figure 8. Schematic illustration of definition of the interface between hydrophilic and hydrophobic regions.

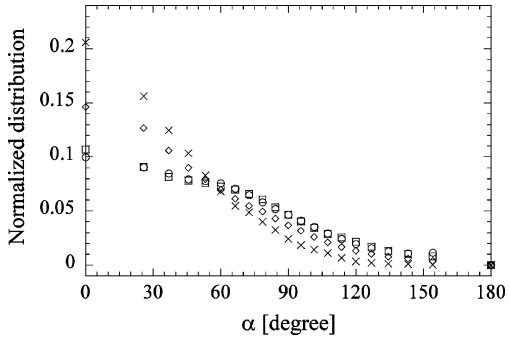

Figure 9. Distribution of the orientational correlation, $\langle \cos \alpha_i(t) \rangle = \langle \mathbf{n}(t) \cdot \mathbf{s}_i(t) \rangle$, between the normal of the interface of hydrophilic and hydrophobic regions (**n**) and the side chain direction (**s**), which was defined as a vector from the end tail of the side chain (CF group) to sulfur atom as shown in Figure 8. The interface was composed of the sulfur of side chain *i* and the nearest two sulfurs, and the normal was set to point from the averaged position of three CF groups, which are end side of the three pendant side chains, toward that of the sulfur atoms. Open circle, square, diamond, and cross are 5, 10, 20, and 40 wt % water swollen membranes, respectively.

hydrophilic and hydrophobic regions with following the equation:

$$\langle \cos \alpha_i(t) \rangle = \langle \mathbf{n}(t) \cdot \mathbf{s}_i(t) \rangle \tag{4}$$

where **n** is normal vector of the interface and $\mathbf{s}_i$ is the direction from the end tail of the side chain (CF group connecting with main chain) to the sulfur of headgroup (see Figure 8). Here, the interface was approximately defined as a plane, which includes the sulfur of the side chain *i* and nearest two sulfurs from it. In addition, the interface normal was set to point from the averaged position of three CF groups, which are the end side of the pendant chains, toward that of the sulfur atoms consisting of the interface. The distribution of time averaged cos α is shown in Figure 9. We can recognize from this result that the pendant side chain inclines to be perpendicular to the interface of hydrophilic and hydrophobic regions. It is also found that the distribution of pendant side chains orientating nearly parallel to the interface normal increases with increase of water uptake ratio. This analysis provides a clear view that the pendant side chains tend to orient perpendicular to the hydrophilic/hydrophobic interface to avoid interacting with water molecules, although the distribution profiles are relatively broad.

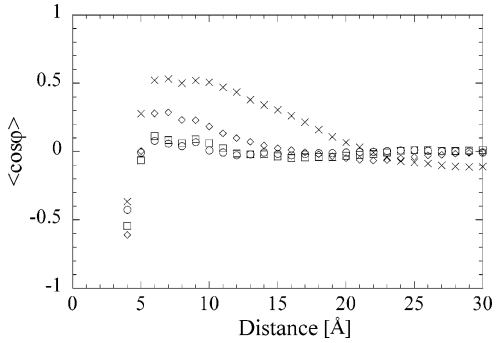

Figure 10. Orientational correlation of the pendant side chains, $\langle \cos \varphi_{ij}(t) \rangle = \langle \mathbf{s}_i(t) \cdot \mathbf{s}_j(t) \rangle$, as a function of the distance between sulfur atoms. The side chain direction **s** was defined as a vector from the end side of the side chain (CF group) to the sulfur atom as shown in Figure 8. Open circle, square, diamond, and cross are 5, 10, 20, and 40 wt % water swollen membranes, respectively.

Figure 10 displays the correlation of the orientations of pendant side chains, *i* and *j*, which is defined as $\langle \cos \varphi_{ij}(t) \rangle = \langle \mathbf{s}_i(t) \cdot \mathbf{s}_j(t) \rangle$, as a function of their distance. One of the notable results is that cos φ is negative in the short range, less than 5 Å. This result demonstrates a possibility of existing of very narrow space, where a few water molecules are sandwiched by the pendant side chains orientating to opposite directions each other. Remarkably, such a situation can be observed even in the 40 wt % water swollen membrane. In the range of about 5−10 Å, the pendant side chains prefer to the analogous direction at all conditions, and the averaged cos φ increases with increase of water content. There is no correlation between the side chains separating over 10 Å at 5 and 10 wt % water swollen membranes, whereas a longer range correlation was observed in 20 and 40 wt % water uptake membranes.

C. Water Cluster. The snapshots in Figure 4 reveal that domain growth or microphase separation of hydrophilic and hydrophobic regions is encouraged with increasing water contents. Figure 5 shows the RDFs of water molecules for four systems. Under low humidity conditions, in the case of 5 and 10 wt %, the first and second peaks in the RDFs are distinguishing, whereas they gradually decrease with increasing water content. To analyze the water cluster size, the structure factors were evaluated as the Fourier transform of the RDFs of water following eq 3 (Figure 6b). Consequently, the membranes under lower humidity conditions, such as 5 and 10 wt %, have their peaks around 0.25 $Å^{-1}$, representing about 2−3 nm size of water aggregation. This should correspond to the typical diffraction peak around 0.11−0.15 $Å^{-1}$ experimentally observed by SANS and SAXS for perfluorinated ionomres,[16,17,20] although the cluster size estimated from our calculations is smaller than experimental one. Possible reasons for such disagreement are due to a shorter polymer chain in our simulation model. The peak intensity increases due to water sorption, and its position shifts toward smaller *q* values, though the peak shapes cannot be completely reproduced for 20 and 40 wt % membranes because of the limitation of the simulation size. These facets indicate water cluster growth due to water uptake, and this view is consistent with experiments.[4,16,17,20] In summary, despite the above limitations, our simulation reasonably reproduces the experimental aspects for size and growth of water cluster, qualitatively.

To elucidate the water cluster dynamics, we analyze the time course of water cluster size. To define the cluster, two sets of cut off distance (R_c) between water oxygen atoms on water, 3.0 and 4.5 Å, are used. These distances are almost the first and second peaks in RDF of water. Figure 11 shows the time

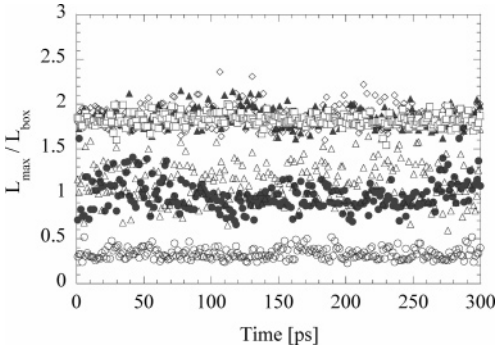

Figure 11. Time courses of the specific length (L_{max}/L_{box}). The length (L_{max}/L_{box}) is obtained by dividing the longest distance between water oxygen atoms belonging to the same water cluster (L_{max}) by the length of simulation cell (L_{box}). Open circle, triangle, square, and diamond are 5, 10, 20, and 40 wt % swollen membranes analyzed with $R_c = 3.0$ Å, and those filled are with $R_c = 4.5$ Å.

courses of the specific length, which is obtained by dividing the longest distance between water oxygen atoms belonging to the same water cluster (L_{max}) by the length of simulation cell (L_{box}). We defined that percolation occurs when L_{max} is longer than L_{box}. As a result, L_{max} is always larger than L_{box} in the case of 20 and 40 wt % swollen membranes, indicating persistent percolation of water under these conditions. In the case of 10 wt % swollen membrane, percolation occasionally occurs when the cut off distance is 3.0 Å, whereas it is always observed for $R_c = 4.5$ Å. On the contrary, in 5 wt % swollen membrane, water percolation frequently arises for $R_c = 4.5$ Å, but never occurs for $R_c = 3.0$ Å. These results suggest that stable water path exists in more humid membrane than 20 wt % water content, and dynamic formation and destruction of continuous water cluster would take place at relatively low humidity. However, it is difficult to estimate the time interval of formation and destruction of continuous water cluster, because it depends on the definition of R_c, although the previous study has concluded that it is roughly 100ps for 17.5 wt % swollen membrane at 298 K.[46]

Next, we tried to categorize the water into three groups defined as follows:

(1) *Free water* (FW): interact with water only within 6.0 Å
(2) *Bounded water* (BW): interact with sulfur within 4.5 Å
(3) *Loosely bounded water* (LW): otherwise

Similar definition has been used to explain the spin−spin relaxation time measured by ^{1}H pulse NMR.[35] The results of analyses are listed in Table 4 and graphically shown in Figure 12. As a result, no FW exits in the dry conditions, such as 5 and 10 wt % swollen membranes, meanwhile the fractions of FWs are 8.3 and 44.1% in the 20 and 40 wt % membranes, respectively. Though the water clusters percolate in the latter two conditions, FWs are continuous only in the case of 40 wt % swollen membrane, as seen in Figure 12. Kim and co-workers have concluded that the ratios of FW, LW, and nonfreezing water (BW) are about 24, 65, and 11%, respectively, for 33% water uptake Nafion-1135 membrane as a result of NMR

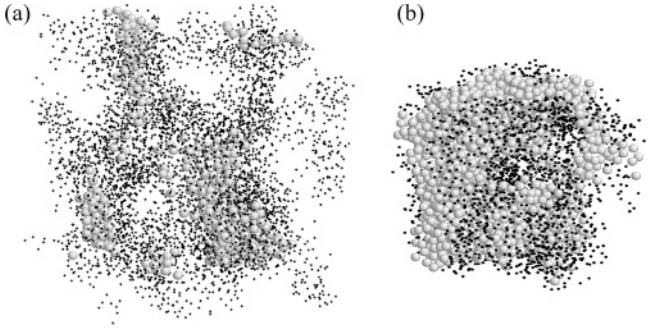

Figure 12. Illustration of free water (FW; gray beads are oxygen of FW), which is defined as waters interacting with only water within 6 Å, in (a) 20 wt % swollen membrane and (b) 40 wt %. Dots represent the position of the other water oxygen.

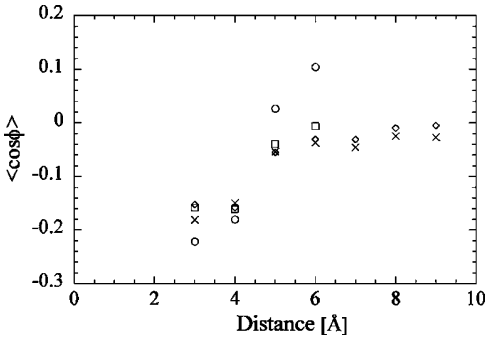

Figure 13. Orientational correlation of water dipole (**d**) against the normal of the interface between hydrophilic and hydrophobic regions (**n**), $\langle \cos \phi_i(t) \rangle = \langle \mathbf{n}(t) \cdot \mathbf{d}_i(t) \rangle$, as a function of the distance between water oxygen and the nearest sulfur atom. Open circle, square, diamond, and cross are 5, 10, 20, and 40 wt % water swollen membranes, respectively.

measurement.[35] Although these values are sensitive to the criterion for the water classification, these two independent investigations provide the comparable results qualitatively.

Water orientation against the hydrophilic/hydrophobic interface was also analyzed in an analogous fashion to the side chain orientation analysis discussed above. Here, we defined water orientation as follows:

$$\langle \cos \phi_i(t) \rangle = \langle \mathbf{n}(t) \cdot \mathbf{d}_i(t) \rangle \quad (5)$$

where **n** is normal vector of the interface and $\mathbf{d}_i$ is the dipole axis of water molecule *i*. The surface was defined by the nearest three sulfurs from a water oxygen atom as shown in Figure 8. Here, we assumed that the inner product of the vector from averaged coordination of the three sulfurs to the water oxygen and the interface normal vector is positive. Figure 13 shows the distance dependence of the water orientation from the nearest sulfur atom. Consequently, it was observed that the dipole axis of water molecule prefer to direct to the polymer matrix in less than 4.0 Å in all conditions. This is because the bounded waters (BWs) should form hydrogen bonding with sulfonic oxygen. On the contrary, the averaged orientation approaches zero with

TABLE 4: Dynamics of Waters Categorized to Free Water (FW), Loosely Bounded Water (LW), and Bounded Water (BW)[a]

water content	ratio (%)			self-diffution coefficient ($\times 10^{-6}$ cm^2/s)			rotational relaxation time (ps)		
	BW	LW	FW	BW	LW	FW	BW	LW	FW
5 wt %	84.5	15.5	0.0	0.07	0.11	-	27.5	21.4	-
10 wt %	73.1	26.9	0.0	0.17	0.22	-	5.6	3.5	-
20 wt %	44.6	47.1	8.3	0.37	0.47	0.62	2.1	1.2	0.6
40 wt %	19.0	36.9	44.1	0.56	0.66	0.77	1.2	0.8	0.5

[a] See text.

TABLE 5: Water Content Dependence of Self-Diffusion Coefficients and Rotational Relaxation

water content	self-diffusion coefficient ($\times 10^{-6}$ cm^2/s)		rotational relaxation time (ps)
	water	polymer	water
5 wt %	0.03	0.002	26.5
10 wt %	0.10	0.008	5.1
20 wt %	0.27	0.016	1.5
40 wt %	0.54	0.072	0.7

separating from the polymer surface, indicating that free water molecules (FWs) uniformly orientated as bulk water.

D. Water Dynamics. The effective diffusion coefficients of water oxygen (D_w) and polymer chain (D_p), and rotational relaxation times of water dipole axis (τ_w) for four different humidity conditions are summarized in Table 5. Herein, the effective diffusion coefficient was evaluated from the mean square displacements as follows:

$$D = \frac{\langle |r(t) - r(0)|^2 \rangle}{6t} \tag{6}$$

On the other hand, the rotational relaxation time was estimated by using the rotational correlation function defined as

$$C(t) = \left\langle \frac{1}{2}[3\cos^2\theta(t) - 1] \right\rangle = \frac{1}{2}\langle 3[d_i(t)\cdot d_i(0)]^2 - 1 \rangle \tag{7}$$

where d_i(t) is the dipole axis vector of water molecule i. The relaxation time was evaluated by using the numerical integration of the correlation function. The tail region of the correlation function is fitted to a single exponential form. The D_w monotonically increases with increasing water content, which indicates that the water in the membrane is strongly localized at a relatively low humidity membrane, and the mobility approaches that of bulk water with increasing water uptake ratio. The same phenomenon was observed by several experiments.[6,34,75] For example, typical diffusion coefficients of water are about (0.5−7.3) $\times$ 10^{-6} cm^2/s for 2−22 H_2O/SO_3 water contents,[6] and (0.129−3.72) $\times$ 10^{-6} cm^2/s for 0.2−1.0 water activities.[75] The former study employed NMR, whereas the latter estimated effective diffusion coefficient from analysis of steady-state permeation combined with equilibrium solubility measurements.[75] Although D_w evaluated from our simulations is smaller than experimental ones, it is safe to say that our MD simulations can reasonably reproduce the experimentally observed values of D_w within the same order. The effective diffusion coefficient of polymer chain is also enhanced by water uptake, although it is by about 2 orders less mobile than water.

Rotational relaxation time of water substantially depends on the water content ratio as shown in Table 5. In the case of low water concentration membranes, 5 and 10 wt %, τ_w is substantially larger than that of bulk water. This result suggests that water is strongly localized in such relatively dry membrane, whereas the water in more highly swollen membranes shows almost the same rotational mobility as bulk water. Zowadzinski et al. have studied ^{2}H NMR relaxation time of water in Nafion 117 at 303 K as a function of water content, and concluded that the rotational relaxation time increases as the water content decreases.[6] In addition, they noted that the water molecules in the fully hydrated membrane ($H_2O/SO_3 = 14$) exhibit similar local mobility to bulk water.[6] Thereby the variation of rotational relaxation time, which is estimated from our simulations as a function of water contents, is consistent with experiment.

Next, we analyzed the water dynamics in three different conditions, such as free water (FW), loosely bounded water (LW) and bounded water (BW), respectively, as defined in the previous section. The water diffusion coefficients and relaxation times are summarized in Table 4. In this case, we place our attention on the short-time water dynamics, because the time scale that water is localized in the same region is very short. Therefore, we utilized short time trajectory data from 3 to 10 ps to evaluate D_M, although the diffusion coefficient is usually calculated from the long time trajectory. As a result, both translational and rotational mobility of FW, which is present only in 20 and 40 wt % swollen membranes, are clearly larger than those of the other two kinds of water. This result reveals that the water locating near the center of water cluster has the same translational and rotational diffusivity as bulk water, whereas the water present at the edges of the cluster is less mobile due to the strong intermolecular interactions with acidic sites. In the case of low humidity conditions, 5 and 10 wt %, τ_w is sufficiently longer for both bounded and loosely bounded waters, compared with their counterparts in high humid conditions. This remarkable result describes that the waters near the sulfonic acid in relatively low humid membranes are strongly bound there, whereas even the waters locating near to sulfonic acid are much less bound in the case of high water content membranes. This is because waters in drier conditions can be bound with several sulfonic acids at the same time, whereas such a situation should be rare in more humid membranes, as discussed in terms of RDF profiles in previous section.

TABLE 6: Residence Time of Water Depending on the Distance from the Nearest Sulnofic Acid (R_s)

R_s (Å)	residence time (ps)			
	5 wt %	10 wt %	20 wt %	40 wt %
2−4	3.2	1.3	0.7	0.6
4−6	1.2	1.1	0.9	0.8
6−8	0.6	0.6	0.8	0.8
8−10	0.4	0.4	0.7	0.7

To make sure the above findings, we also analyzed the residence time of waters in terms of the following the definitions:

$$C(r,t) = \frac{\langle h_i(\Delta r,t)\, h_i(\Delta r,0) \rangle}{\langle h_i(\Delta r,0)\, h_i(\Delta r,0) \rangle} \tag{8}$$

where $h_i(\Delta r,t)$ was defined as unity if the water molecule i is found within the distance Δr from the nearest sulfonic acid in the interval from $t = 0$ to t = t, otherwise $h_i = 0$. We estimated the residence times depending on the distance from the nearest sulfonic acid as listed in Table 6. These were evaluated in the same manner with rotational relaxation time defined as eq 5. Consequently, the residence time of water substantially depends on water content as well as the distance form the nearest acid site. One of the notable observations is that the waters in the range 2−4 Å for 20 and 40 wt % membranes are less bound despite strong attractive interactions with sulfonic acid, and another is that the mobility of waters in more separated range, over 6 Å, is even restricted in the low humid conditions. A possible reason for the former phenomenon is that the water locating near acid sites frequently exchange their position with more separate water, which is as mobile as bulk water. On the contrary, for the latter phenomenon, the restricted mobility of water locating near sulfonic acid would make the other remote waters less mobile. In summary, we can conclude again that only the water in the low humid condition can be sufficiently bound to the sulfonic acid. In other words, the waters in high water concentration membrane rearrange their positions very

frequently. Larger water mobility is expected to lead to higher proton conductivity in the membranes of perfluorinated ionomers.

Conclusion

Molecular dynamics simulation technique was applied to investigate the static and dynamic properties of water and side chain in the swollen membrane of sulfonic type of perfluorinated ionomer. The calculations were carried out for four different water contents, 5, 10, 20, and 40 wt %, at 358.15 K and 0.1MPa with about 56−83 Å of periodic simulation cells. As a result, our calculations reasonably reproduced water dynamics and the size of water cluster compared with experiments, and demonstrated following interesting results. (1) Waters only coordinate to the sulfonic acid, and the other sites of pendant chain hold few water molecules even in relatively high water concentration membranes, indicating that acid sites locate on the surface of water cluster. Consequently, the pendant side chains prefer to orient perpendicular to the hydrophilic/hydrophobic interface, and long-range correlation of side chain orientations is observed at 20 and 40 wt % water uptake membranes. (2) Sulfonic acids aggregate in short range from 4.6 to 7.7 Å with shearing water molecules despite the electrostatic repulsion between them. (3) Stable water percolation was observed for 20 and 40 wt % swollen membranes, whereas dynamic formation and deformation of water path arises in low moisture condition. Free water, which interacts with water only within 6 Å, exists in more than 20 wt % swollen membrane, and it forms continuous paths in 40 wt % water uptake membrane. (4) Water mobility in relatively dry membrane is substantially restricted due to strong attractive interactions with acidic sites. On the contrary, at high water content membranes, even the water locating near sulfonic acid is relatively flexible. The short residence time of the bound water reveals that such water can frequently exchange their position with relatively free water, which locates in center of water cluster, in highly swollen membranes.

Acknowledgment. We thank referees for their helpful advice and discussions to improve this article.

References and Notes

(1) Flemion; Asahi Glass Co., Ltd. http://www.agc.co.jp/english/index.html.
(2) Nafion; DuPont, http://www1.dupont.com/NASApp/dupontglobal/corp/index.jsp.
(3) Aciplex; Asahi Kasei Corporation, http://www.asahi-kasei.co.jp/.
(4) Tant, M. R.; Mauritz, K. A.; Wilkes, G. L. *Ionomers*; Blackie Academic & Professional: Glasgow, Scotland, 1997.
(5) Sumner, J. J.; Creager, S. E.; Ma, J. J.; DesMarteau, D. D. *J. Electrochem. Soc.* **1998**, *145*, 107.
(6) Zawodzinski, T. A., Jr.; Derouin, C.; Radzinski, S.; Sherman R. J.; Smith, V. T.; Springer, T. E.; Gottesfeld, S. *J. Electrochem. Soc.* **1993**, *140*, 1041.
(7) Zawodzinski, T. A., Jr.; Neemn, M.; Sillerud, L. O.; Gottesfeld, S. *J. Phys. Chem.* **1991**, *95*, 6040.
(8) Okada, T.; Moller-Holst, S.; Goreth, O.; Kjelstrup, S. *J. Electrochem. Chem.* **1998**, *442*, 137.
(9) Zawodzinski, T. A., Jr.; Springer, T. E.; Davey, J.; Jestel, R.; Lopez, C.; Valerio, J.; Gottesfeld, S. *J. Electrochem. Soc.* **1993**, *140*, 1981.
(10) Hsu, W. Y.; Gierke, T. D. *Macromolecules* **1982**, *15*, 101.
(11) Fujimura, M.; Hashimoto, T.; Kawai H. *Macromolecules* **1981**, *14*, 1309.
(12) Fujimura, M.; Hashimoto, T.; Kawai H. *Macromolecules* **1982**, *15*, 136.
(13) Gierke, T. D.; Munn, G. E.; Wilson, F. C. *J. Polym. Sci., Polym. Phys. Ed.* **1982**, *19*, 1687.
(14) Roche, E. J.; Pineri, M.; Duplessix, R.; Levelut, A. M. *J. Polym. Sci., Polym. Phys. Ed.* **1981**, *19*, 1.
(15) Heaney, M. D.; Pellegrino, J. *J. Membr. Sci.* **1989**, *47*, 143.
(16) Elliott, J. A.; Hanna, S.; Elliot, A. M. S.; Cooley, D. E. *Macromolecules* **2000**, *33*, 4161.
(17) Gebel, G. *Polymer* **2000**, *41*, 5829.
(18) James, P. J.; Elliott, J. A.; McMaster, T. J.; Newton, J. M.; Elliott, A. M. S.; Hanna, S.; Miles, M. J. *J. Mater. Sci.* **2000**, *35*, 5111.
(19) Lehmani, A.; Durand-Vidal, S.; Turo, P. *J. Appl. Polym. Sci.* **1998**, *68*, 503.
(20) Rollet, A.-L.; Diat, O.; Gebel, G. *J. Phys. Chem. B* **2002**, *106*, 3033.
(21) Porat, Z.; Fryer, J. R.; Huxham, M.; Rubinstein, I. *J. Phys. Chem.* **1995**, *99*, 4667.
(22) Chomakova-Haefke, M.; Nyffenegger, R.; Schmidt, E. *Appl. Phys. A* **1994**, *59*, 151.
(23) Yamamoto, S.; Hyodo, S. *Polym. J.* **2003**, *35*, 519.
(24) Khalatur, P. G.; Talitskikh, S. K.; Khokhlov, A. R. *Macromol. Theory Simul.* **2002**, *11*, 566.
(25) Mologin, D. A.; Khalatur, P. G.; Khokhlov, A. R. *Macromol. Theory Simul.* **2002**, *11*, 587.
(26) Krueger, J. J.; Simon, P. P.; Ploehn, H. J. *Macromolecules* **2002**, 35, 5630.
(27) Paddison, S. J. *Annu. Rev. Mater. Res.* **2003**, *33*, 289.
(28) Paddison, S. J. In *Fuel Cell Technology and Applications*; Vielstich, W., Lamm, A., Gasteiger, H., Eds.-in-Chief; Handbook of Fuel Cell Technology, Volume 3; J. Wiley and Sons: Chichester, U.K., 2003; Chapter 35.
(29) Paddison, S. J.; Pratt, L. R.; Zawodzinski, T. A., Jr. *J. New Mater. Electrochem. Syst.* **1999**, *2*, 183.
(30) Paddison, S. J.; Paul, R.; Zawodzinski, T. A., Jr. *J. Electrochem. Soc.* **2000**, *147*, 617.
(31) Paddison, S. J. *J. New Mater. Electrochem. Syst.* **2001**, *4*, 197.
(32) Paddison, S. J.; Paul, R. *Phys. Chem. Chem. Phys*. **2002**, *4*, 1158.
(33) Meresi, G.; Wang, Y.; Bandis, A.; Inglefield, P. T.; Jones, A. A.; Wen, W.-Y. *Polymer* **2001**, *42*, 6153.
(34) Gong, X.; Bandis, A.; Tao, A.; Meresi, G.; Wang, Y.; Inglefield, P. T.; Jones, A. A.; Wen, W.-Y. *Polymer* **2001**, *42*, 6485.
(35) Kim, Y. S.; Dong, L.; Hickner, M. A.; Glass, T. E.; Webb, V.; McGrath, J. E. *Macromolecules* **2003**, *36*, 6281.
(36) Yoshida, H.; Miura, Y. *J. Membr. Sci.* **1992**, *68*, 1.
(37) Mauritz, K. A.; Fu, R.-M. *Macromolecules* **1988**, *21*, 1324.
(38) Mauritz, K. A.; Yun, H. *Macromolecules* **1988**, *21*, 2738.
(39) Mauritz, K. A.; Yun, H. *Macromolecules* **1989**, *22*, 220.
(40) Mauritz, K. A.; Yun, H. *Macromolecules* **1988,** 22, 4483.
(41) Iwamoto, R.; Oguro, K.; Sato, M.; Iseki, Y. *J. Phys. Chem. B* **2002**, *106*, 6973.
(42) Buzzoni, R.; Bordiga, S.; Ricchiardi, G.; Spoto, G.; Zecchina, A. *J. Phys. Chem.* **1995**, *99*, 11937.
(43) Urata, S.; Irisawa, J.; Takada, A.; Tsuzuki, S.; Shinoda, W.; Mikami, M. *Phys. Chem. Chem. Phys.* **2004**, *6*, 3325.
(44) Vishnyakov, A.; Neimark, A. V. *J. Phys. Chem. B* **2000**, *104*, 4471.
(45) Vishnyakov, A.; Neimark, A. V. *J. Phys. Chem. B* **2001**, *105*, 7830.
(46) Vishnyakov, A.; Neimark, A. V. *J. Phys. Chem. B* **2001**, *105*, 9586.
(47) Commer, P.; Cherstvy, A. G.; Spohr, E.; Kornyshev, A. A. *Fuel Cells* **2002**, *2*, 127.
(48) Spohr, E.; Commer, P.; Kornyshev, A. A. *J. Phys. Chem. B* **2002**, *106*, 10560.
(49) Takamatsu, T.; Eisenberg, A. *J. Appl. Polym. Sci.* **1979**, *24*, 2221.
(50) Morris, D. R.; Sun, X. *J. Appl. Polym. Sci.* **1993**, *50*, 1445.
(51) Shinoda, W.; Mikami, M. *J. Comput. Chem.* **2003**, *24*, 920.
(52) Cui, S. T.; Siepmann, J. I.; Cochran, H. D.; Cummings, P. T. *Fluid Phase Equilib.* **1998**, *146*, 51.
(53) Cui, S. T.; Cochran, H. D.; Cummings, P. T. *J. Phys. Chem. B* **1999**, *103*, 4485.
(54) Li, H.-C.; Mccabe, C.; Cui, S. T.; Cummings, P. T.; Cochran, H. D. *Mol. Phys.* **2001**, *100*, 265.
(55) Jorgensen, W. L.; Chandrasekhar, J.; Madura, J. P. *J. Chem. Phys.* **1983**, *79*, 926.
(56) Neria, E.; Fisher, S.; Karplus, M. *J. Chem. Phys.* **1996**, *105*, 1902.
(57) Becke, A. D. *J. Chem. Phys.* **1993**, *98*, 5648.
(58) Lee, C.; Yang, W.; Parr, R. G. *Phys. Rev. B* **1988**, *37*, 785.
(59) Miehlich, B.; Savin, A.; Stoll, H.; Preuss, H. *Chem. Phys. Lett*. **1989**, *157*, 200.
(60) Fricsh, M. J.; Pople, J. A.; Binkley, J. S. *J. Chem. Phys.* **1984**, *80*, 3265.
(61) Breneman, C. M.; Wiberg, K. B. *J. Comput. Chem*. **1990**, *11*, 361.
(62) Ewald, P. P. *Ann. Phys.* **1921**, *64*, 253.
(63) Urata, S.; Irisawa, J.; Takada, A.; Tsuzuki, S.; Shinoda, W.; Mikami, M. Submitted to *Phys. Chem. Chem. Phys.*
(64) Jorgensen, W. L.; Maxwell, D. S.; Tirado-Rives, J. *J. Am. Chem. Soc.* **1996**, *118*, 11225.
(65) Møller, C.; Plesset, M. S. *Phys. Rev.* **1934**, *46*, 618.
(66) Frisch, M. J.; Trucks, G. W.; Schlegel, H. B.; Scuseria, G. E.; Robb, M. A.; Cheeseman, J. R.; Zakrzewski, V. G.; Montgomery, J. A., Jr.; Stratmann, R. E.; Burant, J. C.; Dapprich, S.; Millam, J. M.; Daniels, A. D.; Kudin, K. N.; Strain, M. C.; Farkas, O.; Tomasi, J.; Barone, V.; Cossi,

M.; Cammi, R.; Mennucci, B.; Pomelli, C.; Adamo, C.; Clifford, S.; Ochterski, J.; Petersson, G. A.; Ayala, P. Y.; Cui, Q.; Morokuma, K.; Malick, D. K.; Rabuck, A.; Raghavachari, K.; Foresman, J. B.; Cioslowski, J.; Ortiz, J. V.; Stefanov, B. B.; Liu, G.; Liashenko, A.; Piskorz, P.; Komaromi, I.; Gomperts, R.; Martin, R. L.; Fox, D. J.; Keith, T.; Al-Laham, M. A.; Peng, C. Y.;, Nanayakkara, A.; Gonzalez, C.; Challacombe, M.; Gill, P. M. W.; Johnson, B.; Chen, W.; Wong, M. W.; Andres, J. L.; Gonzalez, C.; Head-Gordon, M.; Replogle, E. S.; Pople, J. A. *Gaussian 98*; Gaussian, Inc.: Pittsburgh, PA, 1998.

(67) Andersen, H. C. *J. Chem. Phys.* **1980**, *72*, 2384.

(68) Martyna, G. J.; Tuckerman, M. E.; Klein, M. L. *J. Chem. Phys.* **1992**, *97*, 2638.

(69) Martyna, G. J.; Tuckerman, M. E.; Tobias, D. J.; Klein, M. L. *Mol. Phys.* **1996**, *87*, 1117.

(70) Urata, S.; Tsuzuki, S.; Mikami, M.; Takada, A.; Uchimaru T.; Sekiya, A. *J. Comput. Chem.* **2002**, *23*, 1472.

(71) Urata, S.; Tsuzuki, S.; Takada, A.; Mikami, M.; Uchimaru T.; Sekiya, A. *J. Comput. Chem.* **2004**, *25*, 447.

(72) Hunter, E. P. L.; Lias, S. G. *J. Phys. Chem. Ref. Data* **1998**, *27*, 413.

(73) Vila, A.; Mosquera, R. A. *J. Phys. Chem. A* **2000**, *104*, 12006.

(74) Pople, J. A.; Head-Gordon, M.; Raghavachari, K. *J. Chem. Phys.* **1987**, *87*, 5968.

(75) Rivin, D.; Kendrick, C. E.; Gibson, P. W.; Schneider, N. S. *Polymer* **2001**, *42*, 623.